3.3.1 NMR Description for L1-L3 & C1-C3

Mononulcear Dioxomolybdenum Complexes with –ONS Ligands System

Nuclear Magnetic Resonance Spectroscopy is a powerful tool for the identification of organic compounds in conjugation with other spectrometric information. It is also important for the study of organic groups which are coordinated to the metal ions. Hence, the 1H and 13C NMR spectra of the ligands and their Mo complexes were recorded. The numbering scheme adopted for the NMR spectral assignment is shown by the tables above.

The ^{1}H NMR spectra of the ligands exhibits a phenolic (OH) proton resonance at 10.20, 10.30 and 10.55 ppm, respectively. Upon coordination to the Mo atom, the signal for the OH disappeared, indicating the deprotonation of phenolic OH in order to coordinate with the dioxomolybdenum(VI) cation. A sharp band, at *ca.* δ 11.50 is assigned to the proton attached to the nitrogen atom N(8) and N(10). From the crystal structures, it is evident that these protons are involved in hydrogen bonding with adjacent molecules. The hydrogen bonding decreases the electron density around the proton and thus moves the proton absorption to lower field. On top of that, the aromatic proton resonates in the range of 6.88-8.30 ppm. The absence of coupling interaction by N(8) –H due to unavailability of proton on neighbouring atoms render singlet peak for the imine proton. The presence of the electron withdrawing azomethine group near to the C(7) – H proton leads to its resonance at *ca.*8.30 ppm in **L1** and **L2**.

The carbon skeleton of the molecule was identified by recording the decoupled ^{13}C NMR . The ^{13}C NMR spectra of the three ligands, **L1, L2** and **L3** exhibit C-S chemical shift at 178.51, 181.11 and 183.26 ppm, respectively and azomethine carbon C(7) at *ca.* 140 ppm. These two carbons are found to be more deshielded because of the extensive π electron delocalization along the conjugated framework of the carbon skeleton, which reduces the electron density around the carbon atoms. Upon metal complexation, the resonance peaks of these carbons were shifted to lower field.

3.3.2 NMR Description **L4-L9 & C4-C15**

Mononuclear Dioxomolybdenum Complexes with –ONO Ligands System

The ^{1}H NMR spectra of **L4** and **L5**, exhibits -$OH_{phenolic}$ proton resonance at δ 9.32 and δ 12.15 ppm and H_{imine} -C=N resonance at δ 8.43 and δ 8.58 ppm. Upon coordination to the Mo atom, the -OH signal disappeared, which is due to the deprotonation of $OH_{phenolic}$ and the coordination of the oxygen atom to Mo atom. The C(7)-H proton in the ligands is more deshielded due to the presence of electronic effect exerted by the adjacent N atom. The participation of the imine nitrogen in complexation is signaled by the appreciable downfield shift of the azomethine proton signal to δ 8.89 and 8.85 ppm for **C6** and **C7,** respectively. The presence of MeOH **(C4), i**midazole **(C13)**, DMF **(C12)**, HMPA **(C9 & C11)** as donor solvent ligands in the complexes are shown by resonance peaks at δ 3.38, 7.96, 2.89 & 2.73 and 2.50 ppm, respectively.

From the ^{13}C NMR spectra of the ligands, the carbonyl carbon C(9) appears at *ca.* 165 ppm, indicating the downfield shift is due to the conjugative effect of the N-N-C-O core in the hydrazone ligands. In the substituted phenyl ring, different type of aromatic carbons is distinguishable in the ^{13}C NMR spectra. Due to the presence of adjacent carbonyl group, C=O, which is a π electron acceptor, and the extensive electron delocalization in the phenyl ring, the non-protonated carbon, C(10) also resonates at lower field. Upon metal complexation, the resonance peak for the aromatic carbon of the ligands are generally unaffected.

3.3.3 NMR Description **L10-L14 & C16-C24**

Binuclear and Polynuclear Dioxomolybdenum Complexes

Before the interpretation of the NMR spectra of the complexes is preceded, it appears appropriate to comment some points regarding the spectra of the thiosemicarbazone and dihydrazone ligands. The ^{1}H NMR spectra of the ligands, exhibits δ-$OH_{phenolic}$ proton resonance at *ca.* δ 10.33 and δ 10.68 ppm and amide proton, H_{imine} -C=N resonance at *ca.* δ 8.62 and δ 8.45. The broadening of these absorption peaks may have occurred due to the involvement of the protons in intra- and intermolecular hydrogen bonding interaction [61]. The multiplets due to aromatic protons appear in the δ 6.74 – 7.63 region in all the five ligands. Furthermore, the signal appeared at δ 3.41 in **L12** is assigned to the ethylene (–CH_2CH_2-) group proton. Upon coordination to the Mo atom, the -OH signal in the ligands spectra disappeared. This suggested that the thiosemicarbazone and dihydrazone ligands are coordinated to the metal center in enolic phenoxyl oxygen atoms. On the other hand, the participation of the imine nitrogen in complexation is signaled by appreciable downfield shift of the azomethine proton signal (δ 8.75). The downfield shift of these signals is attributable to the drainage of the electron density from nitrogen atom of azomethine group to the Mo atoms [62]. The complexes, **C18** and **C19** show a few signals in the region of δ 7.85 – 8.72 ppm. These signals are attributed to the protons of bipyridyl molecules.

A comparison of the ^{13}C NMR spectra of the ligands and complexes revealed several interesting features. The average position of the resonance due to secondary amido carbonyl carbon atoms is found to have shifted downfield in the complexes.

Some new signals which are present in **C18, C19** and **C24** spectra but not in the spectra of ligands and the rest of the complexes are assigned to various carbon atoms of 4,4-bipyridine. These signals appeared at δ 121 – 154 ppm region. Additionally, it is remarkable to note that **C20 – C24** show signals at 110 ppm regions corresponding to $–CH_2CH_2-$ group, which appear at 120 ppm in uncoordinated dihydrazone. The upfield shift of these signals in the complexes indicates that the electron density at $–CH_2CH_2-$ carbon atoms is increased in the coordinated dihydrazone.

3.4 Electronic Spectra

Table 19: The wavelength of UV and Visible spectra for Mononuclear Complexes.

Ligands/ Complexes	Wavelength (λ) /nm		
	π - π*	**n - π***	**Charge transfer**
L1	251	316, 346	-
L2	262	315, 347	-
L3	268	317, 351	-
L4	291	302, 338	-
L5	292	303, 338	-
L6	293	313, 339	-
L7	262	301	-
L8	241	305	-
L9	261	318, 333	-
C1	267	316	345
C2	258	315	346
C3	268	318	350
C4	269	315	345
C5	277	321	356
C6	292	336	409
C7	268	314	409
C8	278	340	414
C9	279	325	410
C10	276	315	407
C11	270	315	411
C12	272	301	385
C13	275	361	397
C14	266	303	413
C15	267	318	347

3.4.1 Interpretation of UV-Vis Spectra For Mononuclear dioxomolybdenum(VI) Complexes

Electronic absorption bands of the ligands and complexes in $5x10^{-4}$ M DMF are given in table 19. For the ligands, two absorption bands observed at *ca*. 292 and 302 nm are probably due to the *n* to π^* transition of the -C=N- and –C=O- moieties of the ligands[63]. The absorption band at *ca*. 338 nm may be assigned to the n to π^* transition of aromatic rings. The spectra of the complexes shows a broad band at 400 to 410 nm which is assignable to a ligand to metal charge transfer (LMCT) due to the promotion of an electron from the highest occupied molecular orbital (HOMO) of the ligand to the lowest unoccupied molecular orbital (LUMO) of molybdenum atom[64]. Other LMCT bands which are observable around 290 nm and 350 nm can be ascribed to the oxygen to molybdenum and nitrogen to the molybdenum charge transfer transition, respectively. Higher energy bands appearing below 290 nm are due to intra-ligand transition. The absence of d-d transiton absorption band in the visible region confirms the $4d^0$ electronic configuration of Mo(VI) [65].

Table 20: The wavelength of UV and Visible spectra for Binuclear and Polynuclear Complexes

Ligands/ Complexes	**Wavelength (λ) /nm**		
	π - π*	**n - π***	**Charge transfer**
L1	262	315, 347	-
L10	268	317, 351	-
L12	251	291	-
L13	291	302, 338	-
L14	292	303, 338	-
C18	267	313,	346
C19	270	347	405
C20	247	390	404
C21	286	322	398
C22	248	290	387
C23	248	336	387
C24	268	309	493

3.4.2 Interpretation of UV-Vis Spectra For Bi-& Polynuclear dioxomolybdenum(VI)

The electronic absorption bands of the ligands and complexes in $5x10^{-4}$ M DMF with their tentative assigment are given in table 20. The absorption band of the free ligands can be classified into three regions. The absorption region between 250 to 290 nm in the ligands is the characteristic π to π^* transition of benzene rings of the ligands. Two absorption bands observed between 290-350 nm are probably due to *n* to π^* transition of the -C=N- and –C=O- or –C=S- moieties of the ligands [63]. The spectra of the complexes show a broad band at *ca.* 400 nm which is assignable to a ligand to metal charge transfer (LMCT) due to the promotion of an electron from the highest occupied molecular orbital (HOMO) of the ligand to the lowest unoccupied molecular orbital (LUMO) of molybdenum atom[64]. Electronic spectra of the complexes, **C1 – C7,** in DMF display two absorption bands in 293 – 312 nm and 329 – 355 nm region. These peaks may be assigned to oxygen to molybdenum and nitrogen to the molybdenum charge transfer transition, respectively [66-67]. The slight change in λ values within the **L1 – L5** ligands may be due to their difference in electron donating property incited by the nature of the substituents. For instance, **L1, L2** and **L4** are gradually less electron rich, as a result of the presence of chlorine atoms. This makes HOMO of these ligands higher in energy and experienced a red shift [68]. Higher energy bands appearing below 290 nm are due to intra-ligand transition. In general, the electronic spectra for the complexes are dominated by ligand to metal charge transfer (LMCT) and intraligand transitions since Mo(V1) has a $4d^0$ electronic configuration.

3.5 Thermogravimetric Analysis

Table 21 : Thermogravimetric Analysis for Mononuclear Complexes with –*ONS* Ligand

Comp.	Temp. Range (^oC)	Weight lose observed (Calculated)(%)	DSC_{max}(^oC)	Molecules removed	End residue
C1	a) 90 - 170 b) 170 – 700	a) 20.00 (18.00) b) 53.46 (52.42)	169(+) 237 (-)	a) DMSO b) $ClC_6H_3OCHN_2CSNH_2$	MoO_2
C2	a) 100 - 150 b) 150 – 700	a) 15.70(16.88) b) 57.74(55.41)	166(+) 230(-)	a) DMSO b) $ClC_6H_3OCHN_2CSNHC_2H_5$	MoO_2
C3	a) 100 - 150 b) 150 - 600	a) 13.26 (15.30) b) 54.64 (59.60)	176 (+) 217(-)	a) DMSO b) $ClC_6H_3OCHN_2CSNHC_6H_5$	MoO_2

3.5.1 Thermal properties for Mononuclear Dioxomolybdenum(VI) Complexes with ONS Donor Ligands System

Thermogravimetric Analysis (TGA) was performed on **C1, C2** and **C3** in order to measure the amount and rate of change in the weight of the compounds by heating in air at a rate of 20^{o}C per minute due to decomposition (table 21). The complexes undergo average weight loss of 15% from 100^{o}C to 170^{o}C due to the removal of the DMSO as solvent molecule. The TGA curves of the complexes then show a deep plummet in weight beginning from 170^{o}C to 700^{o}C which correspond to the loss of the thiosemicarbazone ligand from the complexes. Above 700^{o}C, a plateau is observed which correspond to the formation of MoO_2 as the final residue. The DSC curves presented an endothermic melting process for all the complexes at 166-176^{o}C followed by decomposition represented by exothermic process at 217 – 230^{o}C. These

complexes presented similar TG profiles resulting in MoO_2 as main residue after two decomposition steps.

Table 22: Thermogravimetric Analysis for Mononuclear Complexes with *–ONO* Ligands

Comp.	Temp. Range (^oC)	Weight lose observed (Calculated)(%)	DSC_{max}(^oC)	Molecules removed	End residue
C4	a) 70 – 110 b) 110 – 320 c) 320 – 700	a) 7.00 (6.79) b) 35.00 (34.39) c) 30.77 (31.42)	- 286(+) 308(-)	a) CH_3OH b) - $NNCOC_6H_4OCH_3$ c) -$OC_2H_5C_6H_3OC$	MoO_2
C5	a) 80 – 120 b) 120 – 300 c) 300 – 700	a) 7.59 (7.04) b) 29.00 (28.47) c) 37.30 (34.50)	 240(+) 353(-)	a) CH_3OH b) – $NNCOC_4H_3O$ c) -$OC_2H_5C_6H_3OC$	MoO_2
C6	a) 50 – 100 b) 150 – 270 c) 270 – 370 d) 370 – 650	a) 3.51(3.41) b) 15.24 (14.77) c) 31.68 (30.87) d) 25.66 (26.52)	- 194 (+) - -	a) H_2O b) DMSO c) -$NNCOC_6H_4OCH_3$ d) - OC_7H_5Cl	MoO_2
C7	a) 170 – 280 b) 280 – 340 c) 340 – 700	a) 15.66 (16.60) b) 30.07 (29.57) c) 26.33 (26.17)	190, 106(+) 317(+) -	a) DMSO b) - $NNCOC_4H_3O$ c) - OC_7H_5Cl	MoO_2
C8	a) 180 – 260 b) 260 – 370 c) 370 – 760	a) 14.92 (15.24) b) 20.84 (21.28) c) 37.00 (37.30)	243(+) 334(+) -	a) DMSO b) -$C_6H_4(OH)_2$ c) –ClC_6H_4CNNCO	MoO_2
C9	a) 150 – 300 b) 300 - 850	a) 42.31 (40.62) b) 39.14 (40.40)	117, 235(+) 323(+)	a) HMPA + DMF b) $ClC_6H_3OCN_2COC_4H_3O$	MoO_2
C10	a) 190 - 280 b) 280 – 300 c) 300 – 750	a) 13.92 (15.34) b) 27.06 (29.00) c) 30.11 (32.08)	195(+) 293(-) -	a) DMSO b) – $OC_2H_5C_6H_3OC$ c) –$NNCOC_6H_4OCH_3$	MoO_2
C11	a) 170 – 300 b) 300 – 850	a) 52.63 (55.53) b) 22.23 (22.80)	151(+) 277(-)	a) HMPA + -$N_2COC_6H_4OCH_3$ b) –$OC_2H_5C_6H_3OC$	MoO_2
C12	a) 160 – 250 b) 250 – 330 c) 330 - 700	a) 13.60 (14.20) b) 32.00 (31.71) c) 30.09 (28.27)	158(+) 240(+) 280(-)	a) DMF b) –$NNCOC_6H_4OCH_3$ c) – $OC_2H_5C_6H_3OC$	MoO_2
C13	a) 130 – 310 b) 310 – 700	a) 46.36 (44.68) b) 30.66 (28.54)	120, 198(+) 279(-)	a) Imidazole + CH_3OH -$NNCOC_6H_4OCH_3$ b) –$OC_2H_5C_6H_3OC$	MoO_2
C14	a) 180-260 b) 260 – 350 c) 350 – 750	a) 18.68 (19.12) b) 31.16 (29.96) c) 26.28 (27.39)	185 (+) 303(-)	a) C_4H_8SO b) -$NNCOC_6H_4OCH_3$ c) –$OC_2H_5C_6H_3OC$	MoO_2
C15	a) 180 – 280 b) 280-370 c) 370 – 700	a) 16.77 (15.48) b) 32.11 (29.56) c) 31.27 (29.60)	177 (+) 212(+) 318(-)	a) DMSO b) –$NNCOC_6H_4OH$ c) –$OC_2H_5C_6H_3OC$	MoO_2

3.5.2 Thermal properties for Mononuclear Dioxomolybdenum(VI) Complexes with ONO Donor Ligands System

Thermogravimetric analysis of the complexes is used to;

(i) obtain information about the thermal stability of these new complexes

(ii) determine the presence of water molecule

(iii) suggest a general scheme for thermal decomposition of these chelates

In the present investigation, heating rate were suitably controlled at $20^{o}C\ min^{-1}$ under nitrogen atmosphere, and the weight loss was measured from 50 to 900 ^{o}C (table 22). All the complexes are stable until 150 ^{o}C except for the cases of **C4, C5** and **C6**, in which the weight loss of 3.51% and 7.00% was observed corresponding to the removal of water and methanol molecules in the compounds. Above this temperature, the TG curves show 3 steps of weight losses. The first step of decomposition in the temperature range of 150 – 250^{o}C involved the removal of solvent molecules (DMSO, DMF, HMPA or imidazole). With further elevation in temperature, a rapid weight loss in the temperature range of 250 – 370 ^{o}C followed by a gradual weigh loss in the temperature range of 370 – 700^{o}C were observed. This process is supported by endothermic effect and subsequent exothermic process as shown in DSC curves. The total decomposition of the second and third stage weight lose may be ascribed to the dissociation of the Schiff base ligand at -C=N- bond before it was removed from the Mo^{2+} core. Decomposition continues until the final residue, MoO_2 is left. Thermal decomposition data of the complexes are given in table

22. In general, the thermal decomposition behaviour of the complexes can be summarized in **scheme 3**:

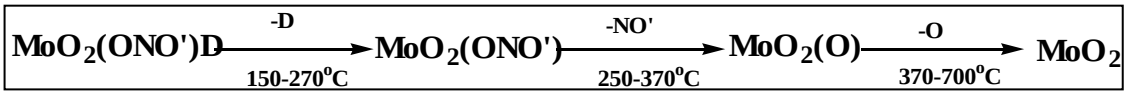

D : Solvent molecules

ONO': Tridentate ligands

Scheme 3: Thermal decomposition of mononuclear dioxomolybdenum(VI) complexes

Table 23 : Thermogravimetric Analysis for Binuclear and Polynuclear Complexes

Comp.	Temp. Range (^oC)	Weight lose observed (Calculated)(%)	DSC_{max}(^oC)	Molecules removed	End residue
C18	a) 200 – 270 b) 270 – 870	a) 15.66 (14.82) b) 72.00 (75.69)	242 -)	a) Bipyridine b) 2 Tridentate ligands	MoO_2
C19	a) 220 – 270 b) 270 – 700	a) 14.32 (16.27) b) 56.54 (60.92)	234 -)	a) Bipyridine N dioxide b) 2 Tridentate ligands	MoO_2
C20	a) 150 – 200 b) 200 – 270 c) 270 – 730 d) 730 – 900	a) 13.44 (11.30) b) 11.35 (11.30) c) 42.12 (44.25) d) 27.78 (31.44)	175 (+) 229 (-)	a) 2 Ethanol b) 2 -OC_2H_5 c) Hexadentate ligands d) $2MoO_2$	-
C21	a) 170 – 200 b) 300 – 350 c) 350 – 620 d) 620 – 870	a) 10.53 (10.62) b) 18.00 (16.40) c) 40.57 (41.57) d) 28.00 (27.45)	160(+) 206(+) 252(-)	a) 2 Ethanol b) 4- Cl c) Hexadentate ligands d) $2MoO_2$	-
C22	a) 100 – 400 b) 400 – 850	a) 42.46 (41.20) b) 30.52 (32.96)	170(+)	a) Hexadentate ligands b) 2 HMPA	MoO_2
C23	a) 150 – 270 b) 270 – 870	a) 19.76 (16.82) b) 52.18 (53.88)	164(+),189(+) 251(-)	a) 2 DMF b) Hexadentate ligands	MoO_2
C24	a) 200 – 280 b) 300 – 874	a) 18.13 (16.50) b) 72.48 (73.32)	251 (+) 270 (-)	a) Bipyridine b) Ligands	MoO_2

3.5.3 Thermal properties of Binuclear and Polynuclear Complexes

The thermal analysis techniques such as thermogravimetry (TGA), differential thermal analysis (DTA) and differential scanning calorimetry (DSC) have been widely applied in studying the thermal behavior of metal complexes. The data enables us to follow a series of structural changes the compounds were subjected to during the thermal treatment, subsequently provided insight pertaining to the thermal stability and thermal decomposition of the compounds in the solid state [69-70].

The TGA analysis of dinuclear tetraoxomolybdenum (VI) complexes have been carried out in the temperature range of 50 to 900 ^{o}C at a heating rate of 20^{o}C min^{-1}. The decomposition stages, temperature ranges, found and calculated weight loss percentage, as well as the thermal effects accompanying the changes in solid complexes on heating are given in the table 23. The thermal behaviour of the mononuclear and binuclear molybdenum complexes is different. For different binuclear complexes, the TGA curves show mass losses in different number of stages which are due to the removal of the solvent molecules and followed by the departure of the ligands. The area of the endothermic DSC peak corresponds to the melting heat while the area of the exothermal peak corresponds to heat of decomposition.

The TGA curve of **C20** shows a mass loss between 150 – 200 ^{o}C, corresponding to an endothermic peak temperature at 175^{o}C, due to the removal of 2 ethanol molecules. The heat of removal of the ethanol molecules obtained from DSC curve (192.81 Jg^{-1}) suggests that the ethanol molecules are loosely attached to the molybdenum center. The second step correspond to the thermal decomposition between 200-270^{o}C which

involve the removal of 2 $–OCH_2CH_3$ fragments from the dihydrazone ligands. This is supported by the exothermic decomposition temperature peak in DSC curve at 229 ^oC and the heat of decomposition calculated (-166.42 Jg^{-1}). Further removal of the hexadentate ligands occurs at higher temperature ranges 270 – 730^oC according to the TGA curve. The final remaining residue, MoO_2 also underwent decomposition at 900^oC.

The thermal decomposition of **C22** undergoes in 2 steps. The departure of the hexadentate ligands takes place between 100 to 400 ^oC with a mass loss of 42.46% (cac. 41.20%). This is supported by the endothermic effect temperature peak in DSC curve at 171^oC and the heat of decomposition calculated (+130.40 Jg^{-1}). The next step between 400 – 850^oC corresponds to the removal of 2 HMPA solvent molecules, leaving MoO_2 as a residue.

The thermal decomposition of **C18** and **C19** undergoes in 2 steps. The removal of the 4,4-bipyridine and 4,4-bipyridine N,N'-dioxide begins at 200^oC and ends at 270^oC. It was observed that the decomposition starts without melting. The DSC curves show the exothermic peak temperature at 242 and 234 ^oC, with ΔH= -48.88 and -320.27 Jg^{-1} respectively. The second stage, which occur in the temperature range 270 – 870 ^oC, correspond to the decomposition of the 2 tridentate ligands from molybdenum atom. The final residue is MoO_2.

The thermal decomposition of **C21** takes place in 4 steps. Two ethanol molecules are removed followed by the fragmentation of chlorine substituted atoms at the salicylaldehyde rings were observed between 170 – 200 ^oC and 300 – 350 ^oC. The third stage is related to the decomposition of hexadentate ligand, taking place in the

temperature range 620 – 870^{o}C. The final residue MoO_2 underwent further decomposition at 620^{o}C. The DSC curve shows two endothermic and one exothermic temperature peak at 160, 206 and 252^{o}C, respectively.

The TGA curve of **C23** shows 2 stages of thermal decomposition. Two molecules of DMF are extirpated between 150 – 270^{o}C. The second stage decomposition which occurs in the temperature range 270 – 870 ^{o}C with the mass loss 52.18% (cal. 53.88%) is accounted for the removal of the hexadentate ligands. The removal of the hexadentate ligands which occur at 251 ^{o}C required 279 Jg^{-1} exothermic heat as shown in the DSC curve. In the case of **C24,** the mass losses (18.13% and 72.48% found) that occurs in two consecutive complicated transition stages in the temperature range 200 – 280^{o}C and 300 – 874^{o}C, respectively, are mainly due to the breakage of 4,4-bipyridine coordinated bond and followed by the decomposition of the dihydrazone ligands.

In general, the fact that various exothermic and endothermic peaks recorded in the DSC curves of the complexes represents a key difference. This difference originates from the packing mode of the complexes. The additional hydrogen bonding interaction in **C18, C19, C20** and **C24** exert more stability to the crystal structure. More precisely, the decomposition of **C18, C19** and **C24** occurred at 200 – 280^{o}C and that of **C22** and **C23** at approximately 100^{o}C. Based on these data, it can be concluded that for the structural transformation in the **C18, C19** and **C24** complexes, which is more stable, larger energy consumption is necessary because of breaking of higher number of intermolecular hydrogen bonding. The thermal decomposition behaviour of the complexes can be summarized in **scheme 4** :

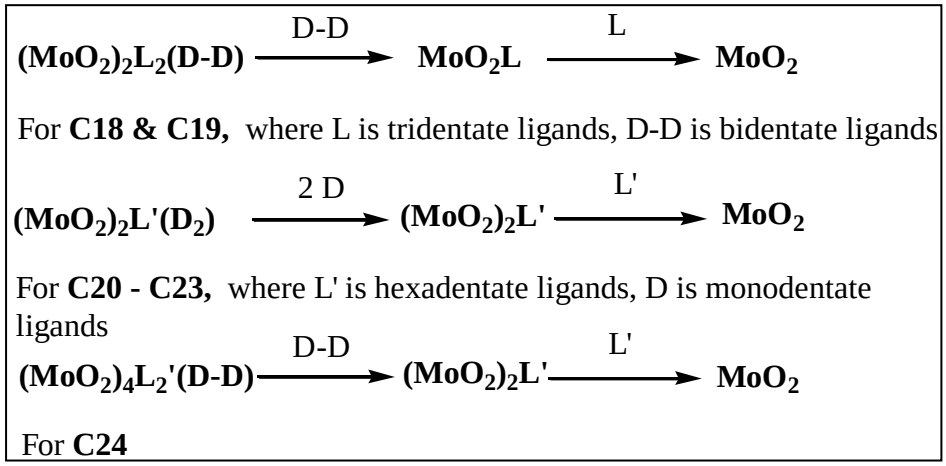

Scheme 4: Thermal decomposition of dinuclear and polynuclear oxomolybdenum(VI) complexes.

3.6 Cyclic Voltammetry Analysis

Table 24: Cyclic Voltammetry Data for Mononuclear Complexes with –ONS Donor Ligands

Compounds	**E_{pc}/V ; (I_{pc}/μA)**	**E_{pa}/V ; (I_{pa}/μA)**
L1	-0.42 (1.28)	-
L2	-0.36 (1.82)	-
L3	-0.37 (1.83)	-
C1	-0.38(1.26), -0.92(3.92)	-
C2	-0.41(1.84) -0.96(3.68)	-
C3	-0.39(1.83) -0.87(2.49)	-

3.6.1 Electrochemical Studies for Mononuclear Complexes with –ONS Donor Ligands

Cyclic voltammetry was used to obtain the cathodic reduction potentials of the mononuclear complexes with –ONS donor ligands at a scan rate of 0.1 Vs^{-1}. Of all of the ligands reported in table 24, only a cathodic reduction peak is observed and no reoxidation was seen at the metal center even as the scan rate was increased. This behavior indicates the irreversible redox process has taken place. The complexes display two reductive responses. The reductive peak at *ca.* -0.38V of the complexes which is close to the reductive response of the corresponding ligand, is attributed to the irreversible reduction of Cl in the ligand. The absence of the metal centered oxidative peak in the complex show that the Mo(V) cannot be oxidized to the

corresponding dioxomolybdenum(Vl) complexes, most likely due to the difficulty in adding a second oxo group to the Mo.

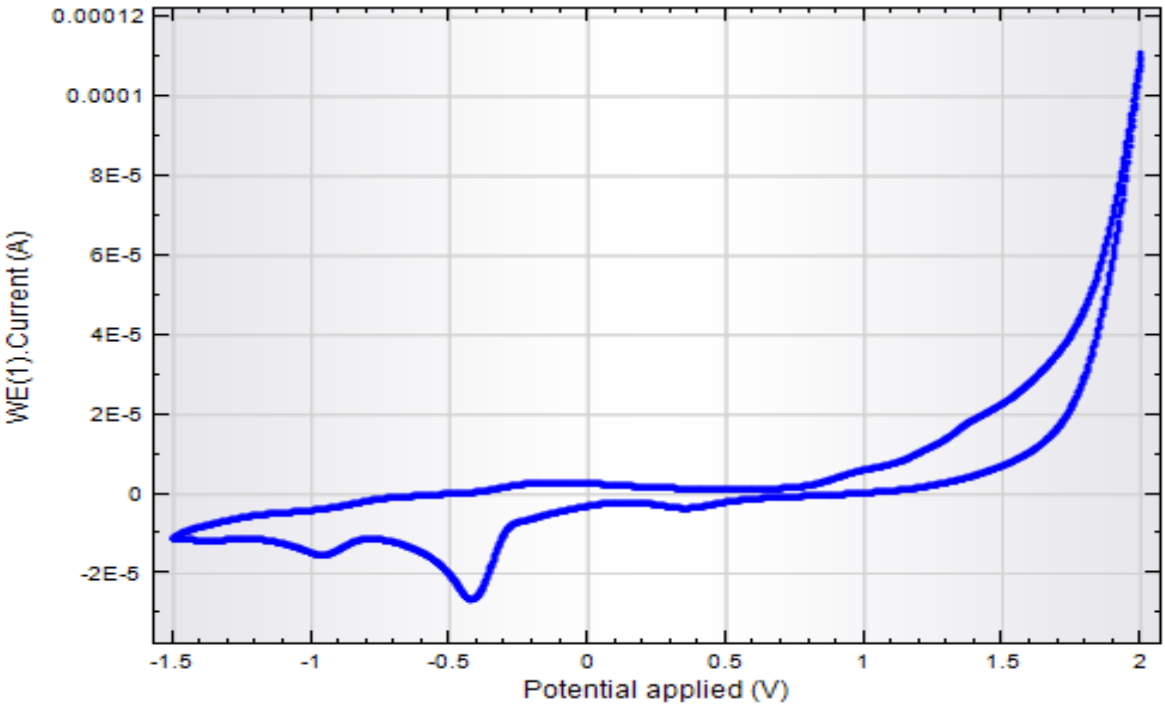

Figure 10: Cydic Voltammogram of C3 in DMF at the rate of 0.1 Vs^{-1}

Table 25: Cyclic Voltammetry data for Mononuclear Complexes with –*ONO* Donor Ligands System

Compounds	**E_{pc}/V ; (I_{pc}/µA)**	**E_{pa}/V ; (I_{pa}/µA)**
L4	-	-0.58 (1.72)
L5	-	-0.51 (2.15)
L6	-1.08 (1.95)	-0.55 (1.90)
L7	-	-0.64 (1.05)
L8	-	-0.55 (1.60)
L9	-	-0.54 (1.21)
C4	-1.15 (0.34)	-0.68 (0.80)
C5	-1.15 (0.46)	-0.65 (0.87)
C6	-0.96 (4.06)	-0.50 (2.00)
C7	-1.11 (0.86), -1.52 (0.46)	-0.54 (0.31),
C8	-1.04 (1.20)	-0.58 (1.23), -0.75 (0.56),
C9	-1.08 (0.03)	-0.49 (0.13), -0.83 (0.60)
C10	-1.18 (1.43)	-0.68 (0.45)
C11	-1.17 (1.10)	-0.63 (0.30)
C12	-1.17 (1.06)	-0.65 (0.37)
C13	-1.17 (0.88)	-0.56 (0.52), -0.88 (0.91)
C14	-0.86 (1.07)	-0.60 (1.67)
C15	-0.85 (1.21)	-0.57 (0.80)

3.6.2 Electrochemical Studies for Mononuclear Complexes with –ONO Donor Ligands

The redox behavior of the ligands and the complexes were examined in DMF solution using cyclic voltammetry at a platinum electrode with 0.1 M tetraethyl ammonium perchlorate (TEAP) as supporting electrolyte. The CV data is tabulated and the selected I vs E profiles are illustrated in table 25. From the data, **L4, L5, L7, L8** and **L9** exhibit an irreversible one oxidative peak around -0.55 V while **L6** shows reversible electrochemical behaviour with the I_{pa}/I_{pc} ratio calculated is 0.97. For a completely reversible one-electron transfer reaction independent of scan rate, a ΔE = 58 mV and a ratio of 1 for anodic and cathodic peak currents are obtainable. For complexes **C4, C5, C6, C10, C11, C12, C14** and **C15,** one oxidative and reductive responses are scrutinized near -0.80 and -1.10 V, respectively. The oxidation wave in these complexes is due to the effect of the redox behaviour of the ligands as the observed values fall in the region as recorded in free ligands. Only the reduction wave in the complexes is attributable to reduction at the molybdenum centers. In the case of **L6** and **C8,** both oxidative and reductive responses appeared approximately in the same region. However, in the case of **C10** to **C13**, the cathodic reduction potential occur around -1.17 V. The more negative the cathodic reduction potential, the more difficult is the dioxomolybdenum(VI) complexes reduced. Both the electron donating groups ($-OC_2H_5$) and the additional aromatic ring for greater electron delocalization in **L8** and **L9** is probably the leading contributor to the shift to more negative values of the cathodic reduction potential in **C10- C13** [71-73a]. From the calculated value of ΔE = 290 mA and I_{pa}/I_{pc} = 1.03 for **C13**, it is to suggest that **C13** undergoes reversible

redox reaction. However, in general, the CV studies on these cis-dioxomolybdenum(VI) complexes revealed irreversible redox behavior.

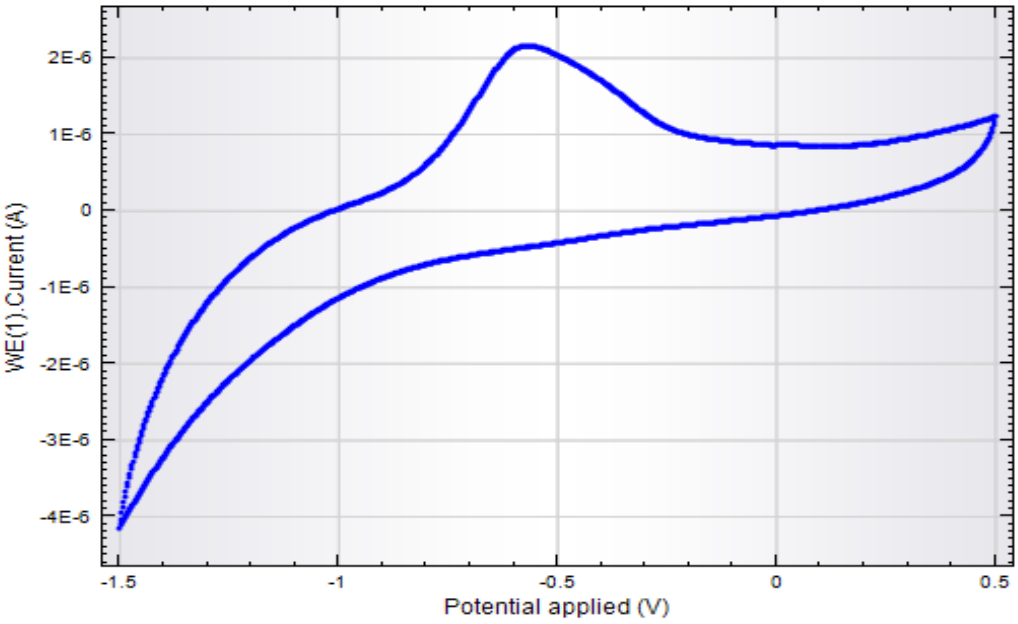

Figure 11: Cyclic Voltammogram of L4 in DMF at the rate of 0.1 Vs^{-1}

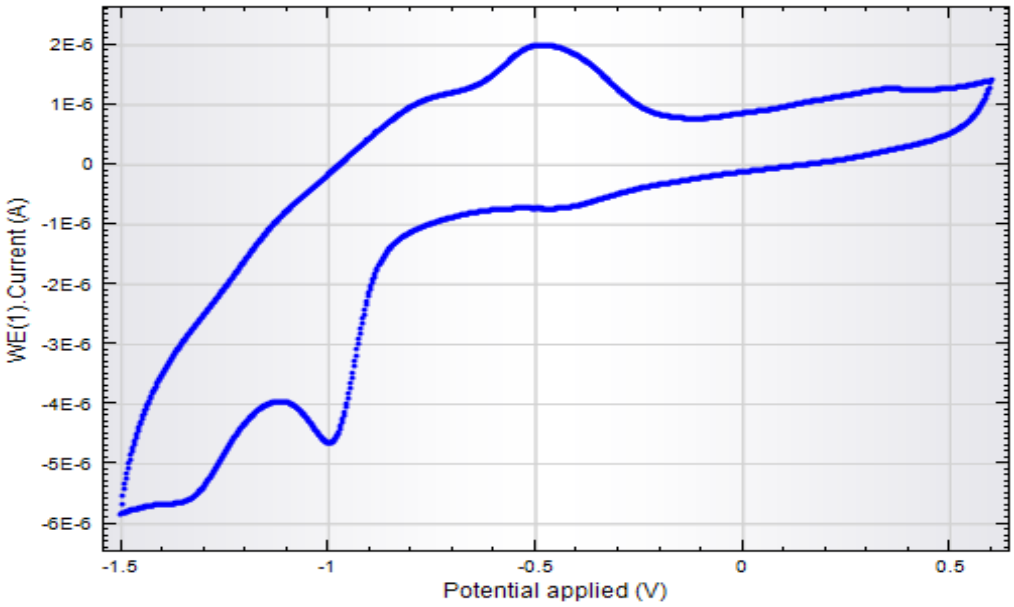

Figure 12: Cyclic Voltammogram of C6 in DMF at the rate of 0.1 Vs^{-1}

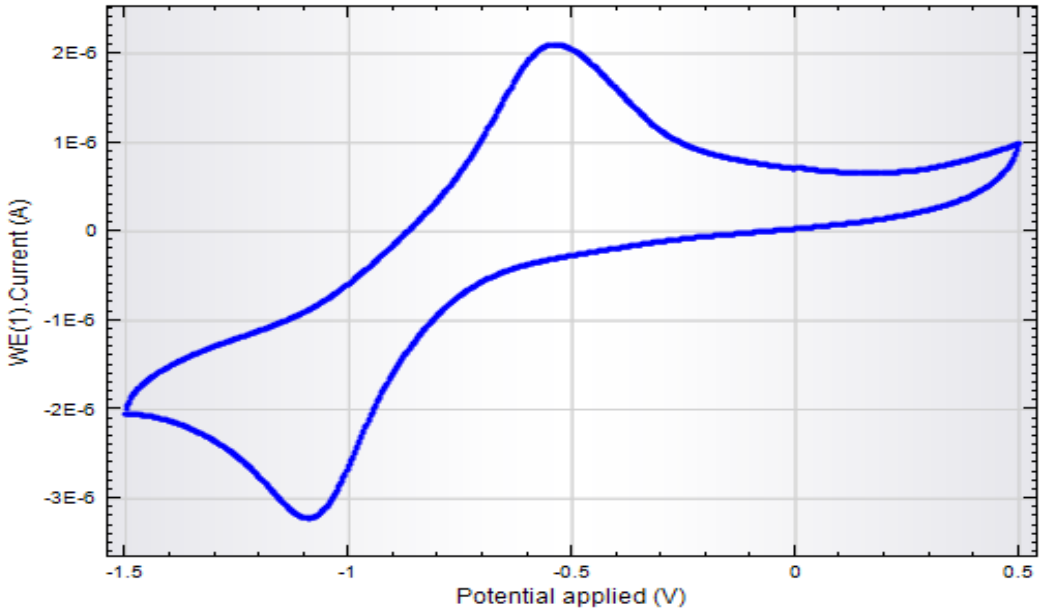

Figure 13:Cyclic Voltammogram of L6 in DMF at the rate of 0.1 Vs^{-1}

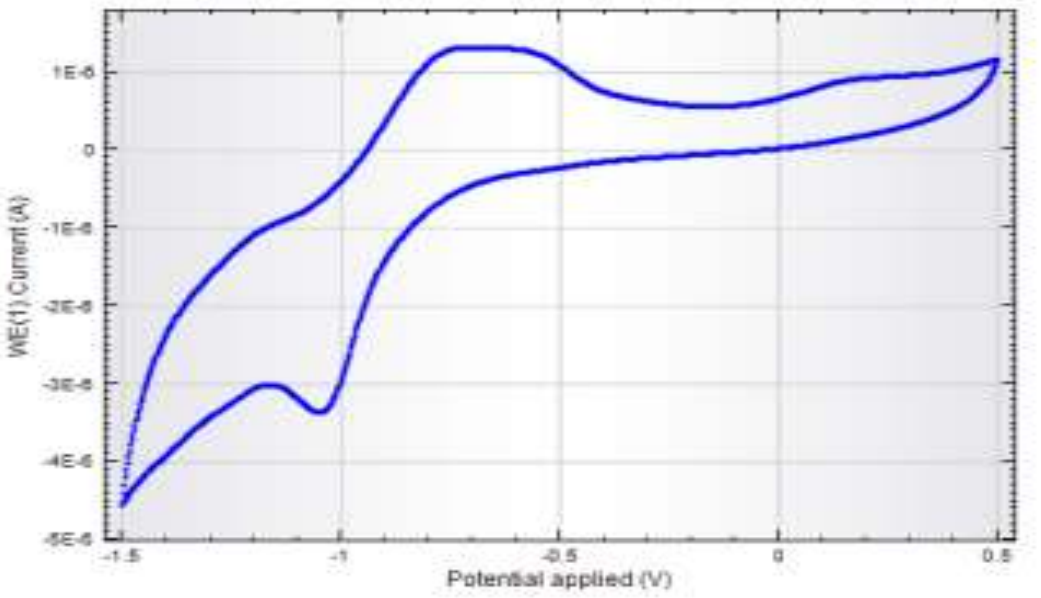

Figure 14: Cyclic Voltammogram of C8 in DMF at the rate of 0.1 Vs-1

Table 26: Cyclic Voltammetry Data for Binuclear and Polynuclear Complexes

Compounds	**E_{pc}/V ; (I_{pc}/µA)**	**E_{pa}/V ; (I_{pa}/µA)**
L10	-0.36 (0.35)	-
L11	-0.38 (0.11)	-0.30 (0.56)
L12	-0.37 (3.90)	-0.28 (5.35)
L13	-0.38 (0.13)	-0.28 (5.09)
L14	-0.49 (0.26)	-
C16	-0.38 (0.13), -0.85 (2.10)	-0.30 (1.23)
C17	-0.39 (0.22) -0.87 (2.32)	-0.27 (0.78)
C18	-0.39 (8.14), -0.94 (2.21)	-0.21 (1.91)
C19	-0.40 (0.23), -0.94 (3.42)	-
C20	-0.38 (0.14), -0.86 (3.45),	-0.29 (5.32)
C21	-0.38 (7.77), -0.85 (3.12)	-0.28 (1.81)
C22	-0.38 (0.11), -0.83 (2.12)	-0.28 (5.64)
C23	-0.38 (0.15), -0.85 (3.68)	-0.29 (5.89)
C24	-0.40 (4.79), -0.86 (1.18)	-0.25 (1.38)

3.6.3 Electrochemical Studies for Dinuclear and Polynuclear Complexes

The redox behavior of the ligands and the complexes were examined in DMF solution using cyclic voltammetry at a platinum electrode with 0.1 M tetraethyl ammonium perchlorate (TEAP) as supporting electrolyte at a scan speed of 0.1 Vs^{-1} (table 26). A comparative study of the cyclic voltammetry behaviour of hydrazones with their metal complexes provides information on whether the redox reaction of the metal complexes is metal centered or ligand centered. From the data, **L11**, **L12** and **L13** exhibit an irreversible one oxidative peak around -0.28 V and one reductive peak at -0.38 V, while **L10** and **L14** show only one reduction peak from -0.36 to -0.42 V, in the cyclic voltammogram recorded in the potential range +2.0 to -1.5 V. The structure (mononucleating ligands and binucleating ligands) as well as the different electron donating property of the substituent groups in the ligands are probably the leading contributor to the additional anodic oxidative potential in **L12** and **L14**. In the case of **C18**, the CV trace of the complexes displays two reductive responses within the potential window -0.39 to -0.94V. The reductive wave at -0.39 V in the complexes is due to the effect of the redox behaviour of the ligands as the observed values fall in the region as that for the free ligands. Only the -0.95 V in the complexes is attributable to reduction at the molybdenum center. The calculated I_{pa}/I_{pc} ratio = 0.81 and 1.17 for **C18** and **C24**, respectively, indicating that these complexes carry reversible redox property. On the contrary, the other type of the dinuclear molybdenum, **C19-C23**, show two successive irreversible one electron oxidation and reduction within -0.25 to -0.86 V. The emergence of these peaks in the complexes could be assigned to

irreversible metal centered and the ligand-centered oxidation and reduction process [51]. Patterson and Holm have shown that softer ligand tend to produce more positive E^o, while hard ligand give rise to negative value of E^o. The more negative reduction potential of **C19** compared **C20 – C23** indicates that Mo ions in the complexes are much more stabilized in higher oxidation state due to the presence of strong and hard donor atoms (N,O) pyridyl and azomethine group in the ligands and solvent coodination [72]. In general, CV studies on these dinuclear and polynuclear molybdenum(VI) complexes reveal that the complexes have essentially similar irreversible redox behaviour, except for **C18** and **C24.**

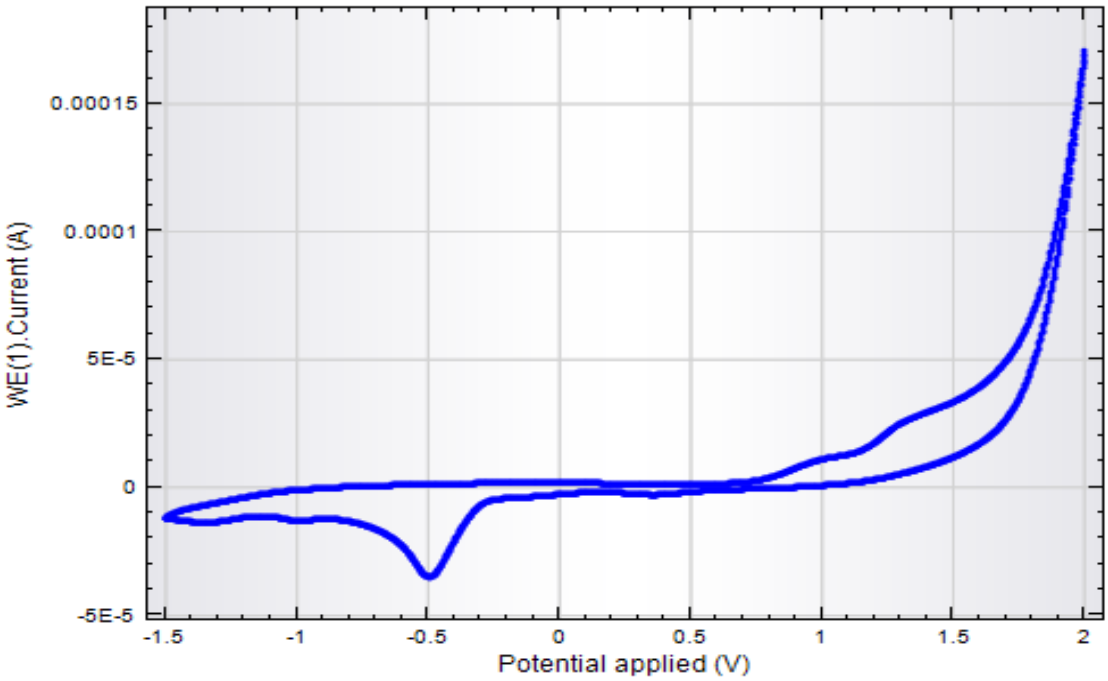

Figure 15: Cyclic Voltammogram of L14 in DMF at the rate of 0.1 Vs^{-1}

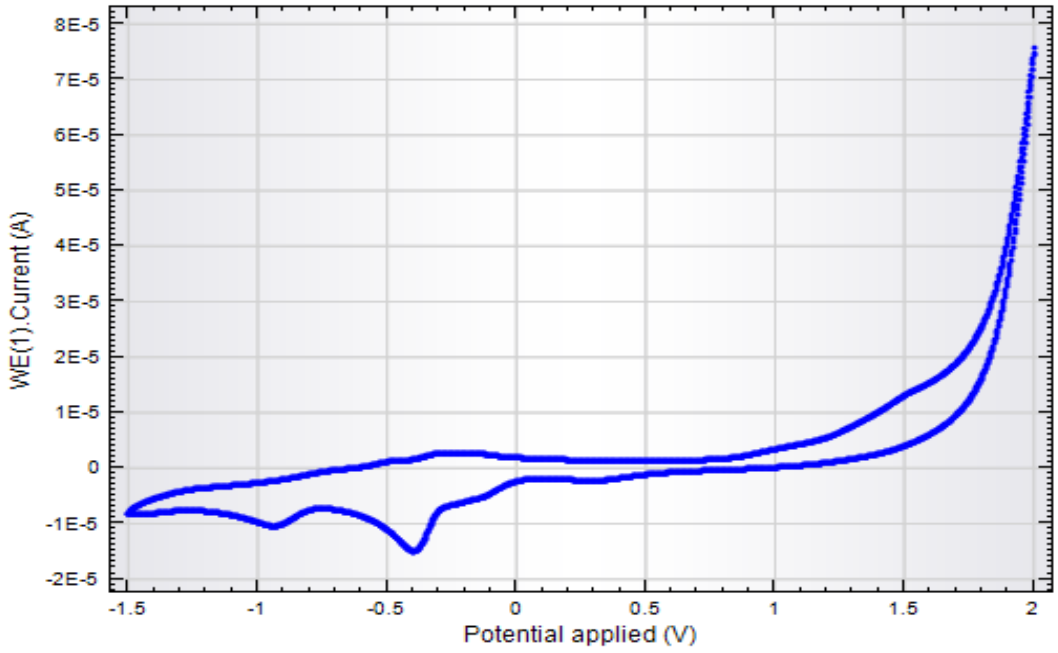

Figure 16: Cyclic Voltammogram of C18 in DMF at the rate of 0.1 Vs^{-1}

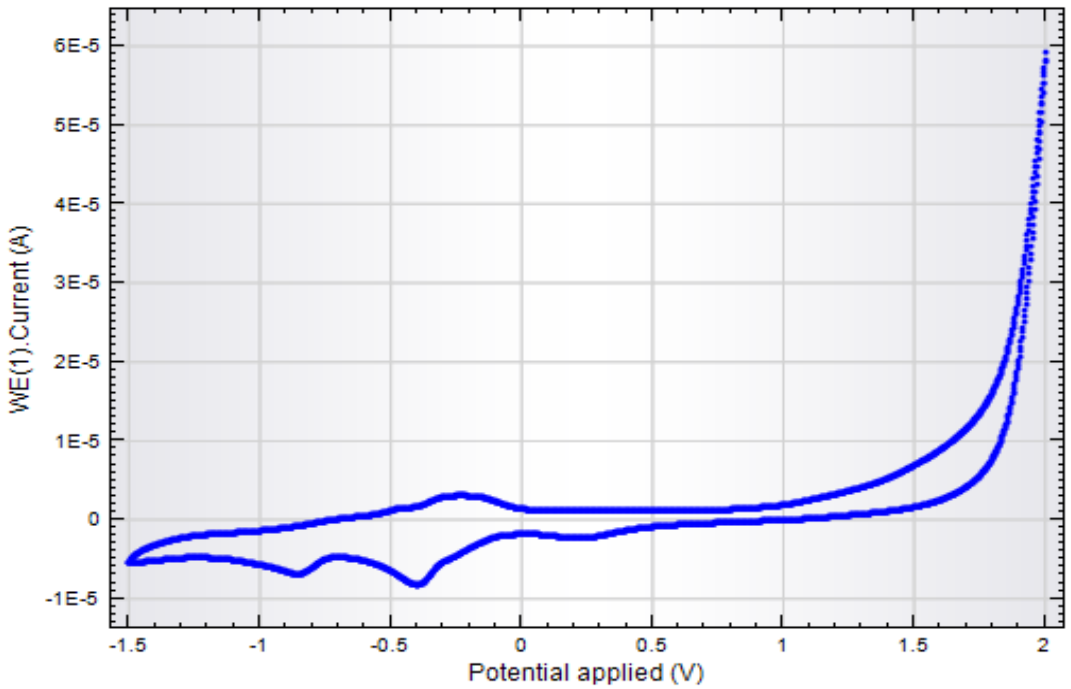

Figure 17: Cyclic Voltammogram of C24 in DMF at the rate of 0.1 Vs^{-}

3.7 Crystal Structures

3.7.1 Introduction

In order to understand the coordination chemistry of oxomolybdenum(VI) complexes, it is necessary to determine their structural characteristic and stability in solid state. With this reason, X-ray structural analysis of the complexes plays an important role not only for the detection of molecular structure, but also the mode of three dimensional packing and overall intermolecular interaction in the complexes.

3.7.2 Crystallographic description of the Mononuclear Dioxomolybdenum(VI) Complexes with –ONS donor ligands system

The molecular structures of **C1, C2** and **C3** show that the Schiff base behave as a tridentate ligand, and reacted with the dioxomolybdenum anion to give a six coordinated molybdenum(VI) structure. As shown in the figures 18-20, the imine nitrogen, one of the phenoxyl oxygen and the sulfur atom are involved in the coordination with molybdenum atom. The *cis*-MoO_2 core is octahedrally surrounded by two terminal oxo-oxygen atoms, the imine nitrogen, phenoxyl oxygen, sulfur atom and finally the oxygen atom from the solvent. In this case, the ligand which coordinates to Mo atom formed six- and five-member chelate rings around the *cis*-MoO_2 centre.

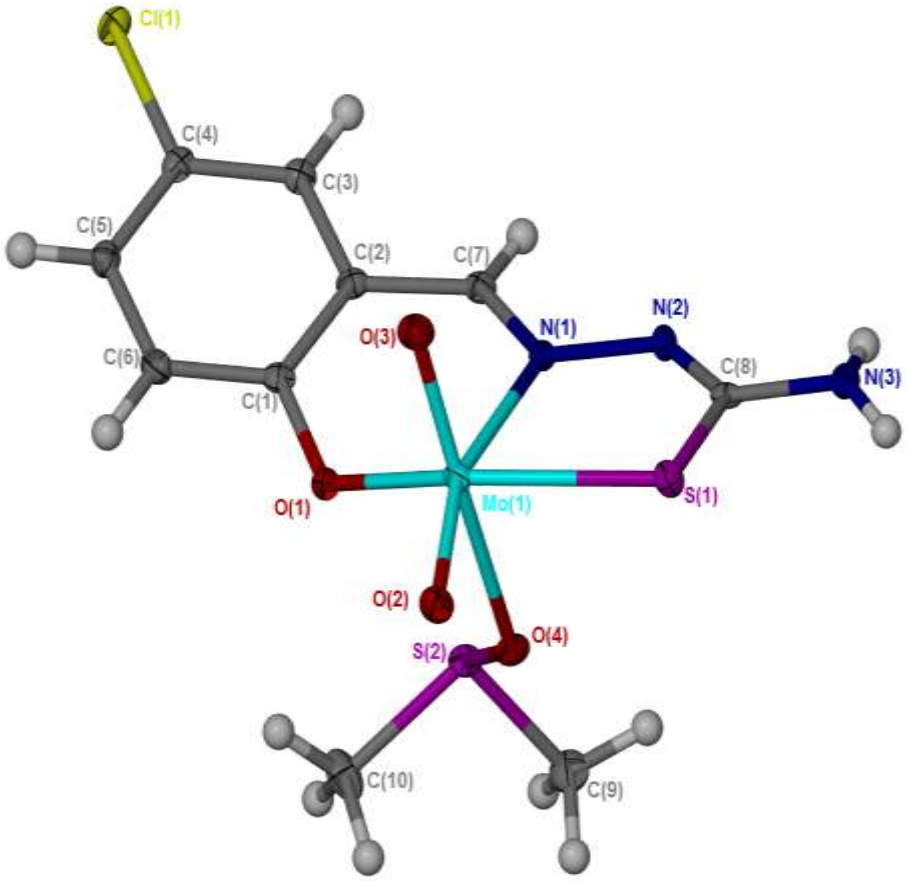

Figure 18: Ellipsoidal plot of C1 with 50% level of probability. The atomic coordinates were given in the Appendix on page 230.